EFFECTS OF MECHANICAL PROPERTIES OF MATERIAL ON CRATERING: A LABORATORY STUDY

By J. Burlin Johnson and R. L. Fischer

* * * * * * * * * * * report of investigations 6188

US Department of Interior
Office of Surface Mining
Reclamation and Enforcement

Kenneth K. Eltschlager
Mining/Blasting Engineer
3 Parkway Center
Pittsburgh, PA 15220

Phone 412.937.2169
Fax 412.937.3012
Keltschl@osmre.gov

UNITED STATES DEPARTMENT OF THE INTERIOR
Stewart L. Udall, Secretary

BUREAU OF MINES
Marling J. Ankeny, Director

This publication has been cataloged as follows:

Johnson, J Burlin

Effects of mechanical properties of material on cratering: a laboratory study, by J. Burlin Johnson and R. L. Fischer. [Washington] U.S. Dept. of the Interior, Bureau of Mines [1963]

24 p. illus., tables. 27 cm. (U. S. Bureau of Mines. Report of investigations, 6188)

Bibliography: p. 24.

1. Blasting. I. Fischer, R L joint author. II. Title. III. Title: Cratering. (Series)

TN23.U7 no. 6188 622.06173

U. S. Dept. of the Int. Library

CONTENTS

	Page
Summary	1
Introduction	1
Acknowledgments	1
Testing methods	2
Shear wave velocity (V_s)	2
Bar velocity (V_B)	2
Longitudinal velocity (C)	2
Apparent porosity (P)	4
Specific gravity (ρ)	5
Static tensile strength (T)	5
Static compressive strength	6
Dynamic Young's modulus (E)	6
Dynamic modulus of rigidity (μ)	6
Dynamic Poisson's ratio (ν)	6
Experimental procedure	8
Experimental data	8
Analysis of data	13
Crater depth	13
Crater volume	13
Crater radius	18
Interrelationship of physical properties	18
Conclusions	18
References	24

ILLUSTRATIONS

Fig.		
1.	Resonance testing instrument	3
2.	Point load tensile testing apparatus	4
3.	Schematic of point load tensile testing apparatus	5
4.	Poisson's ratio as a function of different velocity ratios	7
5.	Scaled crater depth vs. scaled charge depth	12
6.	Maximum scaled crater depth vs. physical properties	14
7.	Scaled crater volume vs. scaled charge depth	15
8.	Maximum scaled crater volume vs. physical properties	16,17
9.	Scaled crater radius vs. scaled charge depth	19
10.	Maximum scaled crater radii vs. physical properties	20
11.	Plots of measured physical properties against each other	21-23

TABLES

1.	Cratering materials	9
2.	Physical properties of materials tested	10
3.	Crater test data	11

EFFECTS OF MECHANICAL PROPERTIES OF MATERIAL ON CRATERING: A LABORATORY STUDY

by

J. Burlin Johnson[1] and R. L. Fischer[2]

SUMMARY

This report describes an investigation of the relationship between crater dimensions formed in laboratory blasting experiments and the mechanical properties of the material cratered. Scaled field data have been included when available. The results show that tensile strength and possibly other mechanical properties may be useful in predicting maximum crater dimensions.

INTRODUCTION

The purpose of this Bureau of Mines investigation was to determine to what extent crater dimensions are influenced by some of the commonly measured mechanical properties of the material cratered and to permit a better comparison between laboratory-scale craters and large-scale craters in the field. In an earlier report (2)[3] it was shown that small-scale cratering in mortar in the laboratory resembles large-scale cratering in rock. Furthermore, cube root of charge weight scaling yielded crater dimension curves which were very similar to those obtained with much larger charges in the field. However, it was not possible to make a thorough comparison because equipment for measuring physical properties was not available at the Minneapolis laboratory at that time.

ACKNOWLEDGMENTS

The authors are indebted to D. R. Reichmuth of the Mining Engineering Department, University of Minnesota, for information on his tensile testing technique, for his tensile strength data on the Bedford limestone, and for valuable discussions on physical property measurements in general. They are also indebted to G. H. McLaughlin of Newmont Exploration Ltd. for furnishing details on the sonic resonance instrument, described herein.

[1] Former geophysicist, Minneapolis Mining Research Center, Bureau of Mines, Minneapolis, Minn .

[2] Physicist, Minneapolis Mining Research Center, Bureau of Mines, Minneapolis, Minn.

[3] Underlined numbers in parentheses refer to items in the list of references at the end of this report.

Work on manuscript completed July 1962.

TESTING METHODS

The methods of measuring and computing the values of the mechanical properties of the materials cratered are described below. The testing procedures were somewhat different from those described by Obert, Windes, and Duvall (4).

Shear Wave Velocity (V_s)

The shear wave velocity was determined by the conventional torsional resonance technique with the instrument shown in figure 1. The sample was driven by a phonographic cutting head and audio oscillator, and the resonant frequency was detected and displayed by a phonographic pickup head, amplifier, and oscilloscope. A digital frequency meter was used to measure the resonant frequency to better than 1 percent. This instrument was very convenient to use in that no pole pieces needed to be cemented on or compensating corrections made. The instrument was verified by performing tests on duraluminum and steel bars having known elastic constants. As shown in figure 1, the heads were oriented to drive and to detect torsional resonance. The shear wave velocity is then

$$V_s = 2f_tL$$

where f_t is the torsional resonant frequency, and L is the length of the sample.

Bar Velocity (V_B)

The bar velocity was determined with the same resonance instrument by orienting the heads to drive and to detect longitudinal resonance. Then

$$V_B = 2f_1L$$

where f_1 is the longitudinal resonant frequency. One limitation was that the cutting head used would only respond up to about 14 kilocycles, requiring the use of a fairly long core when high-velocity material was being tested.

Longitudinal Velocity (C)

The velocity of longitudinal elastic waves was determined by measuring the traveltime of an ultrasonic pulse through a specimen. An 800-volt step pulse having a rise time of approximately 0.2 μ sec. was used to excite a piezoelectric source transducer 0.050 inch thick. A similar transducer was used to detect the pulse. The traveltime was measured in several disks and cylinders of different lengths of each material, and the velocity was obtained by least squares from the slope of the time-distance line.[4]

---

[4] Pauline Virciglio, Bureau of Mines mathematician, was responsible for the statistical and computational work in this report.

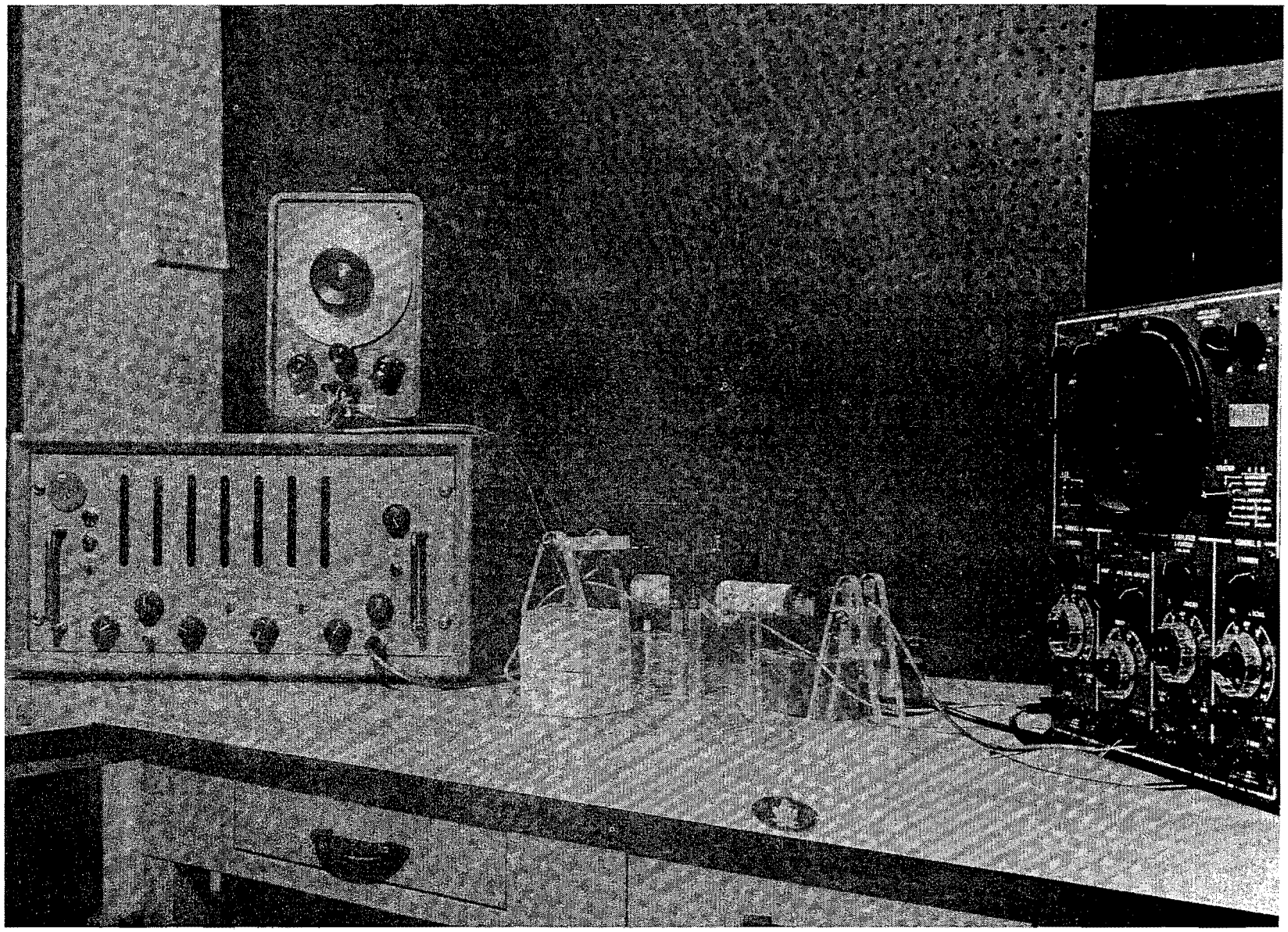

FIGURE 1. - Resonance Testing Instrument.

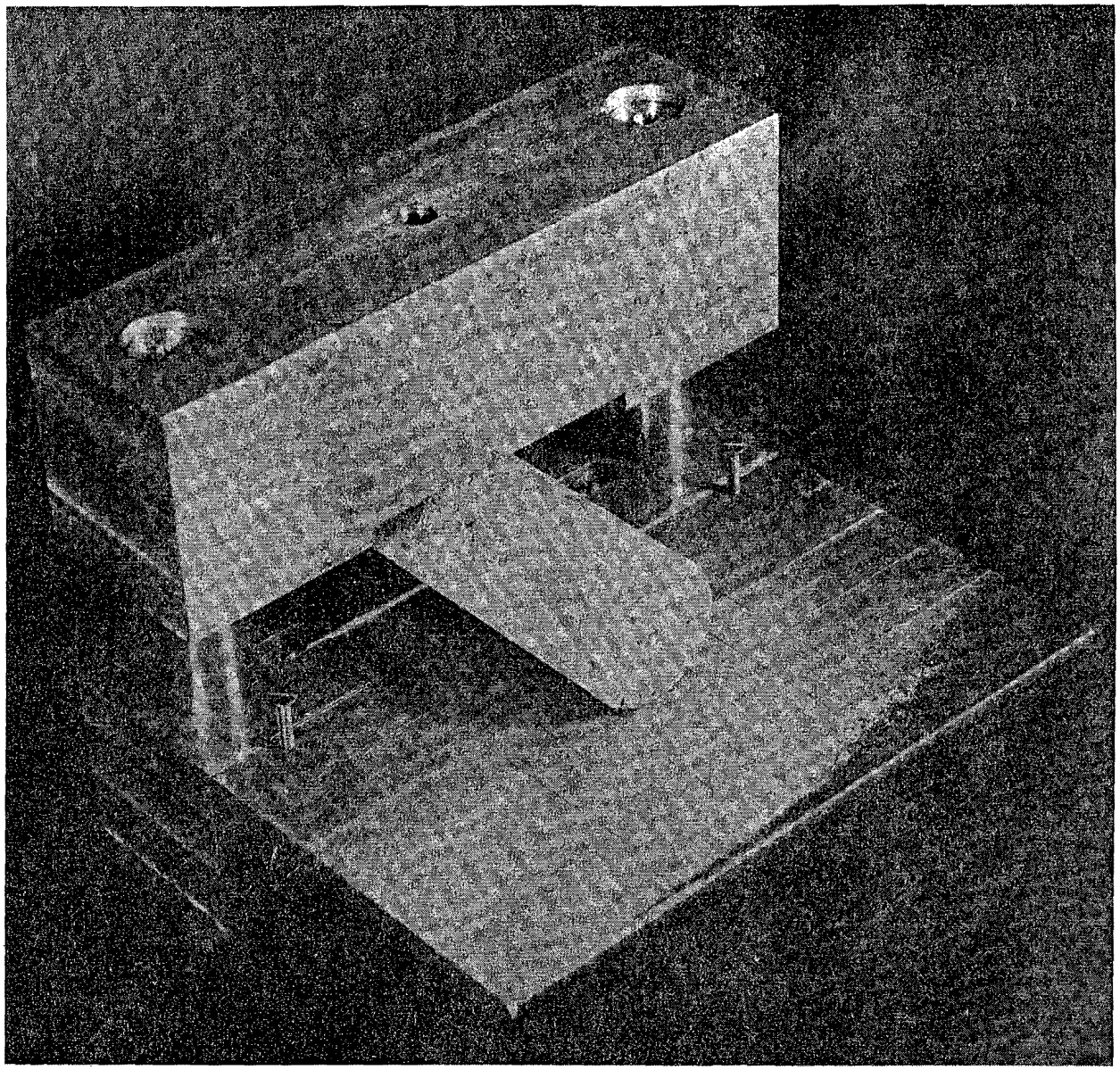

FIGURE 2. - Point Load Tensile Testing Apparatus.

Apparent Porosity (P)

The apparent porosity is defined as the ratio of the volume of open pore space to total volume of the specimen. A gas pycnometer was used to measure the open-pore-space volume. Then

$$P = \frac{V_t - V_p}{V_t} \times 100$$

where V_t is the total external volume, and V_p is the sample volume measured in a gas pycnometer.

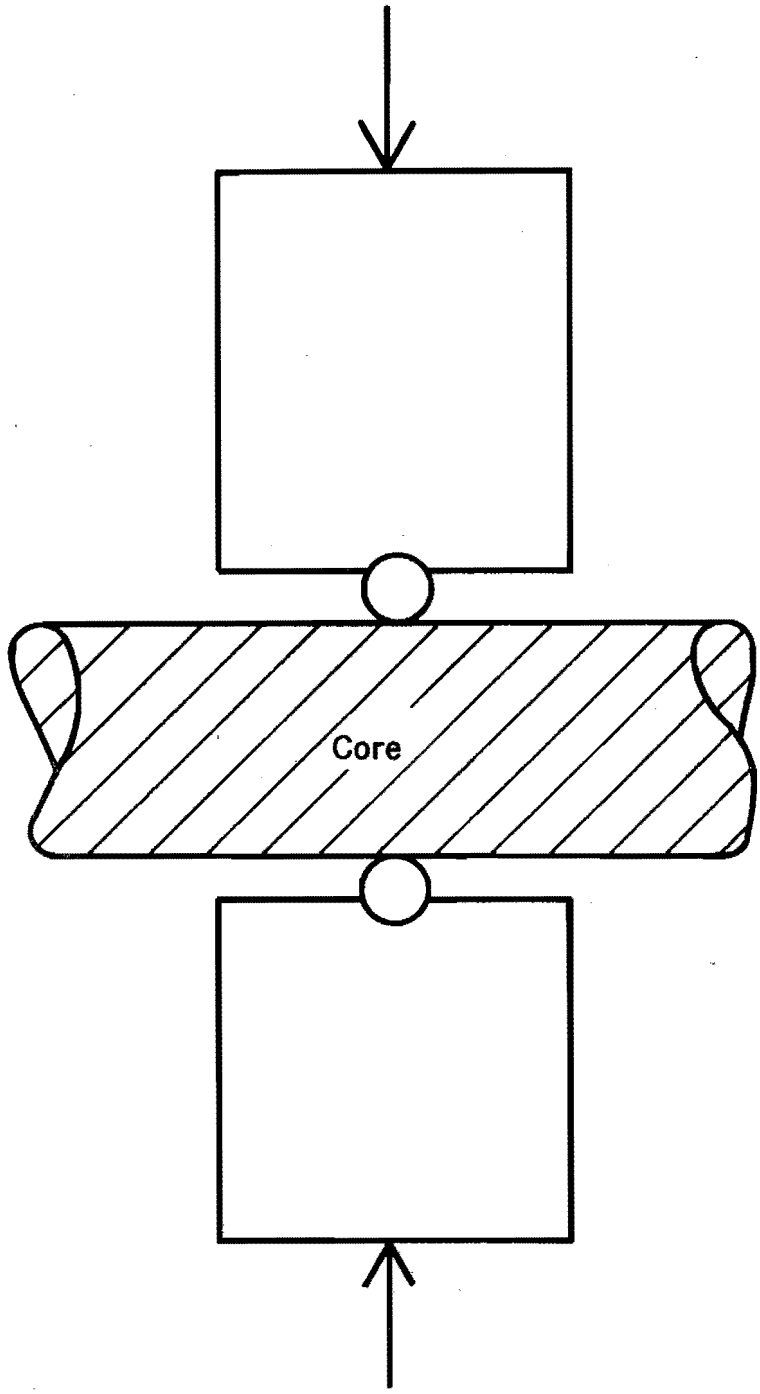

FIGURE 3. - Schematic of Point Load Tensile Testing Apparatus.

Specific Gravity (ρ)

The specific gravity was determined by dividing the weight of the air-dried specimen by the exterior volume of the specimen.

Static Tensile Strength (T)

Tensile strengths were obtained by a method developed by D. R. Reichmuth which consists of applying a point load at the surface of a cylindrical specimen perpendicular to the specimen axis (5). Theory predicts that tensile stresses will exist at the axis when a load is applied in this manner. Reichmuth has shown experimentally that the tensile strength can be computed from the relationship

$$T \cong 0.96\frac{F}{d^2}$$

where F is the breaking force applied, and d is the sample diameter. For diameters of less than 2 inches, the above equation is accurate to better than 10 percent when compared to data obtained by conventional methods such as axial tension or line loading of a cylinder. His method has the advantages that large numbers of tests can be performed rapidly on a limited amount of core, that flaws and weaknesses in the sample have practically no effect unless they lie directly between the applied point loads, and that surface irregularities due to drilling have no effect. A photograph and schematic of the instrument appear in figures 2 and 3. A compressive load was applied perpendicular to the jaws.

Static Compressive Strength

This test was performed in the conventional manner on specimens having a length to diameter ratio of at least 1.75. The ends of the cores were lapped before testing.

Dynamic Young's Modulus (E)

The dynamic Young's modulus was computed, using the measured values of ρ, C, and V_s in the expression

$$E = k \frac{\rho V_s^2 \left[3\left(\frac{C}{V_s}\right)^2 - 4\right]}{\left(\frac{C}{V_s}\right)^2 - 1}$$

where k depends on the units used, and also using the expression

$$E = k \rho V_B^2$$

Dynamic Modulus of Rigidity (μ)

The dynamic modulus of rigidity was computed from the expression

$$\mu = k \rho V_s^2$$

Dynamic Poisson's Ratio (ν)

The dynamic Poisson's ratio was obtained graphically from plots of the following relationships:

$$\nu = \frac{\left(\frac{V_s}{C}\right)^2 - \frac{1}{2}}{\left(\frac{V_s}{C}\right)^2 - 1}$$

$$\nu = \frac{1}{4}\sqrt{\left[1 - \left(\frac{V_B}{C}\right)^2\right]\left[9 - \left(\frac{V_B}{C}\right)^2\right]} - \left[1 - \left(\frac{V_B}{C}\right)^2\right]$$

Although these are not independent determinations, their agreement does afford a check on the proper choice of resonant frequencies used to determine V_s and V_B.

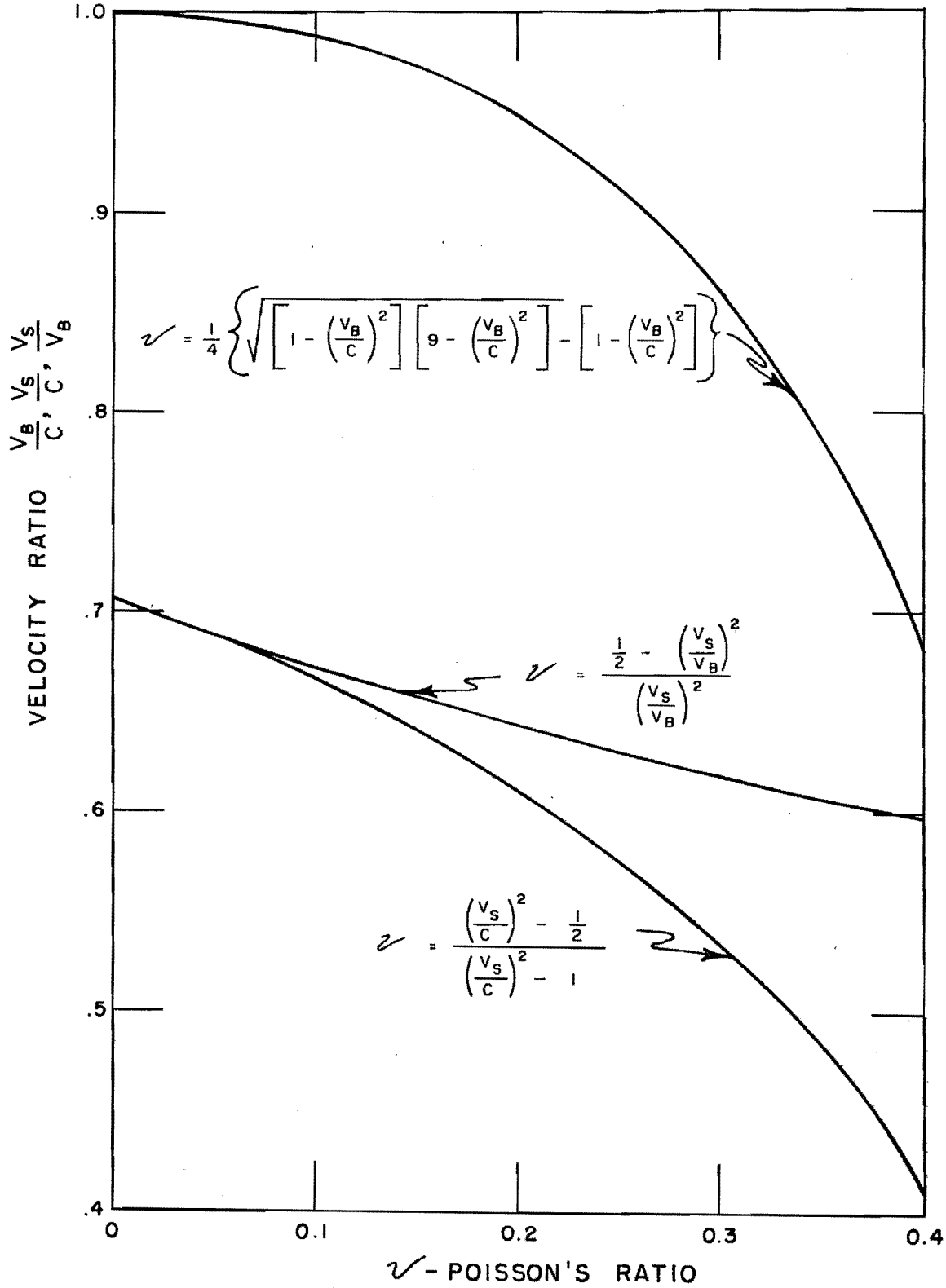

FIGURE 4. - Poisson's Ratio as a Function of Different Velocity Ratios.

This method is considerably superior to the commonly used:

$$\nu = \frac{\frac{1}{2} - \left(\frac{V_s}{V_B}\right)^2}{\left(\frac{V_s}{V_B}\right)^3}$$

For a given error in velocity ratio (and $\nu > 0.1$), the expressions involving $\frac{V_B}{C}$ and $\frac{V_s}{C}$ give a smaller error in ν than the expression involving $\frac{V_s}{V_B}$.

Plots of the three expressions make this readily apparent (fig. 4).

EXPERIMENTAL PROCEDURE

The crater experiments were performed in a manner essentially identical to those described in an earlier report (2). The materials used were mortar, plaster of Paris, limestone, granite, basalt, and candle wax.

The physical properties of all but the wax were determined from cores drilled from blocks of the materials. The mortar and plaster cores were drilled out of the cratered block and were tested within 48 hours of cratering to minimize any aging effects. The wax properties were determined from molded cores. A detailed description of the materials is given in table 1.

The explosive used in all tests was one No. 6 electric blasting cap. The cap was detonated at the bottom of a 5/16-inch shothole stemmed to the top with water-saturated sand. Crater depth, radius, and volume were measured and recorded for each test.

The linear dimensions were scaled by dividing by a scale factor defined as a length in feet numerically equal to the cube root of the charge weight in pounds. For a No. 6 blasting cap this factor is 1.1 inches. For crater volume the factor is 20 cc.

The synthetic materials tested were in the form of blocks 2 by 2 by 1 feet. The rock specimens cratered were in blocks of various shapes. Specimens to be tested were air-dried. Crater volumes were measured after all loose material had been removed from the craters.

EXPERIMENTAL DATA

The physical properties of the materials cratered are given in table 2. For plaster of Paris, it was only possible to obtain one usable core for measuring bar velocity and shear velocity. This same core was used in the single compressive strength test.

The values of Young's modulus obtained by both methods of computation are listed in the table. The value used was the average. The listed value of Poisson's ratio is an average of the two values obtained by using $\frac{V_s}{C}$ and $\frac{V_B}{C}$.

TABLE 1. - Cratering materials

The following blocks were included in the cratering series:

Mortar I.....	Consisted of a mixture of 2 parts sand, 1 part high-early-strength cement, and .50 parts water by weight. The measured specific gravity of the quartz sand was 2.67. When cratered, the block had aged 46 days. All blocks were water cured for 5 days.
Mortar II.....	A strong, lightweight-aggregate mixture; it had an aggregate/high-early-strength cement/H_2O ratio of 2:1:.53. The lightweight aggregate had a specific gravity of 2.45. The age of the block was 63 days.
Mortar III.....	A weak, lightweight-aggregate mixture; it contained the same aggregate as Mortar II and consisted of 6 aggregate/high-early-strength cement/.92 H_2O. The age of the block was 21 days.
Plaster of Paris.....	Block contained 2 quartz sand/1 plaster/.50 water by weight. The aging time was 61 days.
Bedford limestone..... (Bedford, Ind.)	Rounded, cryptocrystalline, carbonate detritus and some crystalline-vein carbonate and numerous, disseminated cavities.
Charcoal granite..... (St. Cloud, Minn.)	Dark, fine-grained granite having the following composition: 66 percent feldspar, 16 percent quartz, 13 percent amphibole, 3 percent biotite, 2 percent miscellaneous.
Rockville granite..... (St. Cloud, Minn.)	Coarse-grained, granite porphyry having the following composition: 65 percent feldspar, 24 percent quartz, 10 percent biotite, 1.0 percent miscellaneous.
Basalt..... (St. Croix Falls, Wis.)	Diabasic texture. Composition: 50 percent feldspar, 40 percent augite, 8 percent magnetite, 2 percent miscellaneous.
Candle wax.....	Block consisted of 165 pounds of candle wax, which was melted and poured into a prepared mold. The resulting block was cratered 14 days later.

TABLE 2. - Physical properties of materials tested

	Mortar I	Mortar II	Mortar III	Plaster of Paris	Bedford limestone	Charcoal granite	Rockville granite	Basalt	Candle wax
Shear velocity, ft./sec.....	7,170	6,100	5,480	5,680	7,480	10,000	10,600	11,900	2,560
No. samples tested.....	9	5	3	1	6	7	9	6	5
Standard deviation.....	177	106	174	-	202	80	243	36	33
Bar velocity, ft./sec.....	11,100	9,760	8,890	8,820	11,500	14,600	16,500	19,100	4,220
No. samples tested.....	1	2	2	1	5	7	5	6	5
Standard deviation.....	-	-	-	-	413	217	251	33	26
Longitudinal velocity, ft./sec....	14,500	12,300	10,300	8,900	13,100	18,800	20,600	21,700	6,640
No. samples tested.....	4	4	11	5	24	20	10	18	12
Tensile strength, p.s.i.....	646	504	249	181	510	1,800	1,340	2,290	51.7
No. samples tested.....	33	14	13	4	33	100	28	22	12
Standard deviation.....	86	46	57	25	49	192	202	304	11.5
Compressive strength, p.s.i.....	7,620	4,300	1,680	1,340	7,680	28,400	19,400	35,700	365
No. samples tested.....	2	5	5	1	13	4	7	12	7
Standard deviation.....	-	735	180	-	725	1,270	3,040	4,625	41.4
Porosity (apparent), percent.....	15.4	26.3	28.9	28.7	15.4	0.77	0.73	0.20	1.17
No. samples tested.....	4	4	4	3	11	3	2	7	5
Standard deviation.....	2.6	1.9	2.5	2.6	0.80	0.04	-	0.063	0.19
Specific gravity.....	2.11	1.73	1.64	1.80	2.30	2.72	2.67	2.96	0.89
No. samples tested.....	8	4	4	4	17	7	4	13	6
Standard deviation.....	0.03	0.03	0.03	0.04	0.022	0.004	0.005	0.013	0.007
Young's modulus, $F(\frac{V_S}{C})$, p.s.i., x 10^{-6}	3.92	2.33	1.72	1.80	4.38	9.56	10.86	14.51	0.22
Young's modulus, $F(V_B)$, p.s.i., x 10^{-6}	3.51	2.22	1.75	1.89	4.11	7.83	9.81	14.58	0.21
Modulus of rigidity, p.s.i., x 10^{-6}.....	1.46	0.87	0.66	0.78	1.74	3.67	4.05	5.65	0.079
Poisson's ratio.....	.35	.34	.30	.10	.27	.32	.32	.28	.41

Included on some of the graphs are data obtained from publications by Duvall and Atchison (1) and Nichols, Hooker, and Duvall (3). Cratering from which this data was gained was done in the field with charges ranging from 0.4 to 32 pounds. The physical property data for these field tests were obtained by using the standardized tests (4) on cores in the laboratory. The values of compressive strength pertaining to the field data were obtained from cores having a length to diameter ratio of 1.0, rather than greater than 1.75. Crater test data for laboratory cores are presented in table 3.

TABLE 3. - Crater test data

Charge depth, in	Crater radius, in	Crater depth, in	Crater volume, cc
Mortar I			
0.4	1.2	0.6	15
.6	1.2	.5	21
.9	1.3	.6	23
1.1	1.9	.6	68
1.4	2.0	.6	45
1.6	2.4	.5	73
1.9	3.7	.6	206
2.3	(1)	(1)	(1)
Mortar II			
0.4	1.2	0.4	11
.9	1.6	.8	35
.9	1.8	.6	31
1.4	2.3	.8	77
1.9	3.1	.6	87
2.1	3.6	.6	177
2.4	(1)	(1)	(1)
2.8	(1)	(1)	(1)
Mortar III			
0.1	1.3	0.6	19
.4	1.6	.9	42
.9	1.9	1.4	86
1.3	2.0	1.1	112
1.7	2.5	1.0	130
2.1	3.0	1.5	267
2.6	4.6	1.9	(2)
2.8	(1)	(1)	(1)
Plaster of Paris			
-0.1	0.5	0.3	0.5
0.5	1.2	.4	14
.9	1.5	.8	43
1.5	2.0	1.0	102
1.9	2.8	1.3	227
2.1	3.5	1.1	286
2.5	(1)	(1)	(1)
Charcoal Granite			
0.4	1.9	0.4	25
.9	1.6	.4	16
1.4	2.4	.4	68
1.9	1.1	.3	8
3.1	.5	.1	1
Bedford Limestone			
0.1	0.8	0.2	3
.3	1.1	.3	7
Bedford Limestone (Con.)			
0.6	1.2	0.5	15
1.1	1.5	.6	18
1.4	1.9	.6	70
1.5	2.3	.6	44
1.7	1.8	.6	50
1.8	(3)	(3)	(3)
1.9	2.9	.6	111
1.9	1.0	.6	9
1.9	1.7	.4	18
2.1	0.9	.3	4
2.2	1.0	.3	7
2.4	0.6	.2	1
2.8	(1)	(1)	(1)
Rockville Granite			
0.3	1.3	0.3	11
.6	1.7	.4	21
.9	2.6	.4	50
1.2	1.9	.4	35
1.6	1.4	.4	16
1.6	2.6	.6	61
2.3	1.9	.5	28
2.3	1.9	.5	27
2.8	0.7	.3	2
3.1	.8	.3	2
3.4	.6	.3	2
3.9	(1)	(1)	(1)
Basalt			
0.1	1.0	0.3	4
.7	1.4	.3	17
1.1	1.4	.4	17
1.9	1.0	.3	10
2.6	1.0	.3	6
2.9	1.0	.3	8
3.1	(3)	(3)	(3)
Candle Wax			
-0.1	0.4	0.4	1
0.1	.9	.8	9
.4	1.6	.9	43
.8	1.7	1.2	56
1.9	2.7	0.8	176
2.4	4.4	1.4	715
2.9	(1)	(1)	(1)

[1]No crater. [2]Not measured. [3]Broken block.

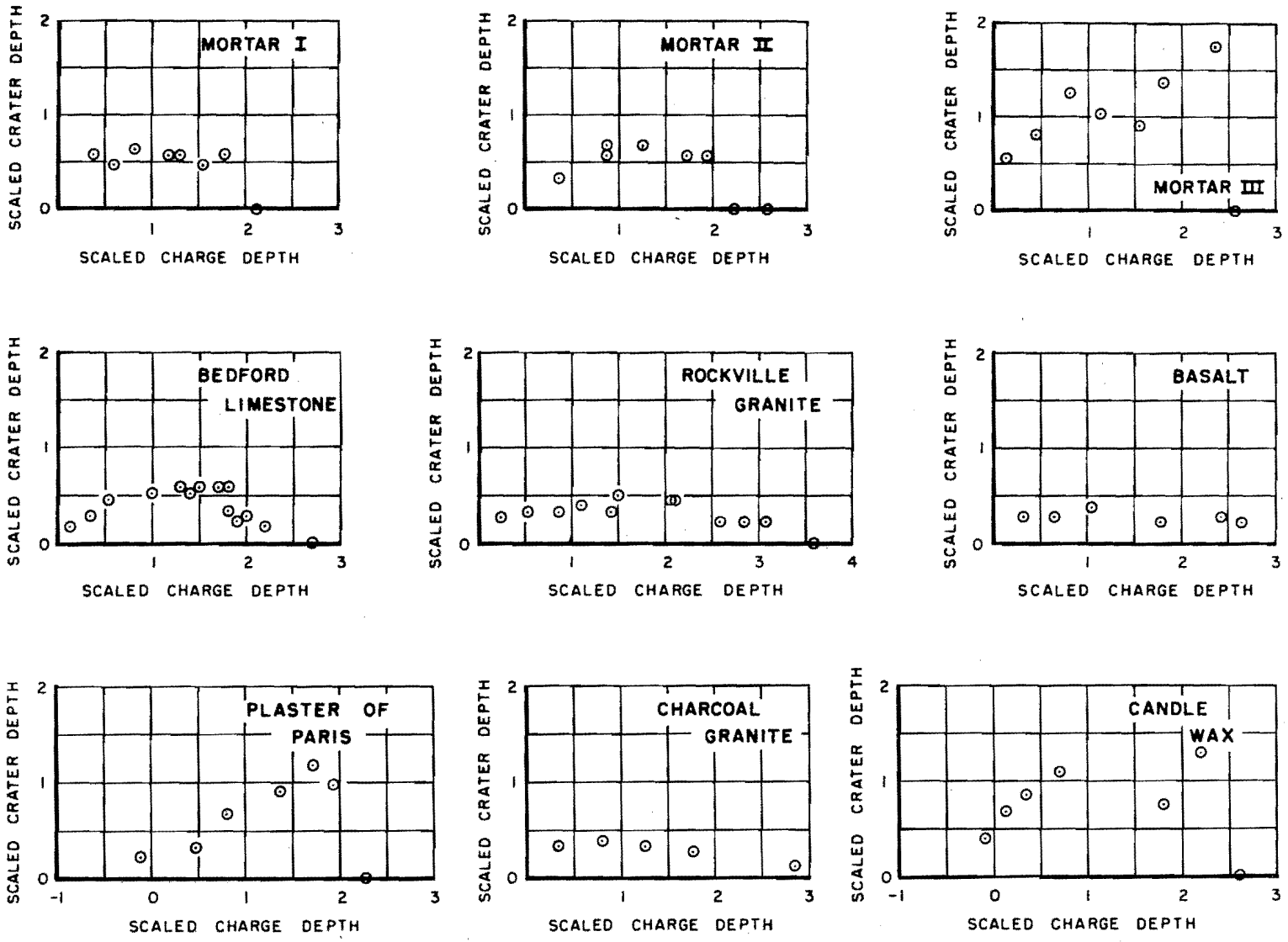

FIGURE 5. - Scaled Crater Depth vs. Scaled Charge Depth. (Scaled crater depth and scaled charge depth are in ft/lbs$^{1/3}$.

ANALYSIS OF DATA

Crater Depth

Scaled crater depth as a function of scaled charge depth is shown in figure 5. It is interesting that scaled crater depth remains relatively constant for most materials in the scaled charge depth range of about 0.5 to 2.0. For all materials there are cases where the scaled charge depth is greater than the scaled crater depth. When the crushed zone around the charge is all beneath the bottom of the crater, it is clear evidence that the reflected strain pulse is responsible for the crater formation. Where the crushed zone around the charge is large and reaches the bottom of the crater, the mechanism is less clear. This latter condition occurred in the mortar III and plaster of Paris blocks.

The marked effect of strain pulse attenuation is also apparent from inspection of the graphs. Cratering occurs at scaled charge depths greater than 3 in Rockville granite. A similar result probably would have been obtained in charcoal granite and basalt, where data are incomplete due to an insufficient amount of suitable rock. These materials are characterized by high modulus of elasticity, sonic velocity, and strength. The weaker materials, in which larger craters were formed, would not crater at scaled charge depths greater than 1.8 to 2.4.

Plots of maximum scaled crater depth against the various physical properties for both laboratory and field tests are shown in figure 6.

The plot showing the least scatter is that of tensile strength. This is not surprising, if the reflected strain pulse is the main cause of cratering. In fact, tensile strength is quite likely the most important property in most types of failure of brittle material. Because this property was measured at low rates of loading, whereas cratering occurs at high rates of loading, the plot implies a fairly simple relationship between dynamic and static tensile strength. It should be noted, however, that due to the shape of the curve, this relationship is not too useful for predicting the maximum crater depths.

Trends occur in all the plots except that of Poisson's ratio, and in general they are improved considerably by excluding one or more field data points. This is understandable in that cores are not nearly as representative of the rock blasted in the field as they are of rock blasted in the laboratory where the core volume is the same order of magnitude as the crater volume.

Crater Volume

Scaled crater volume versus scaled charge depth is shown in figure 7. Most of these plots show an exponential increase in crater volume as crater depth is increased, up to a maximum, after which crater volume drops rapidly to zero. The granite and basalt data are an exception to this.

The relationships between maximum crater volume and the various mechanical properties are shown in figure 8. Since small changes in charge depth near the optimum depth can cause fairly large changes in crater volume, one would

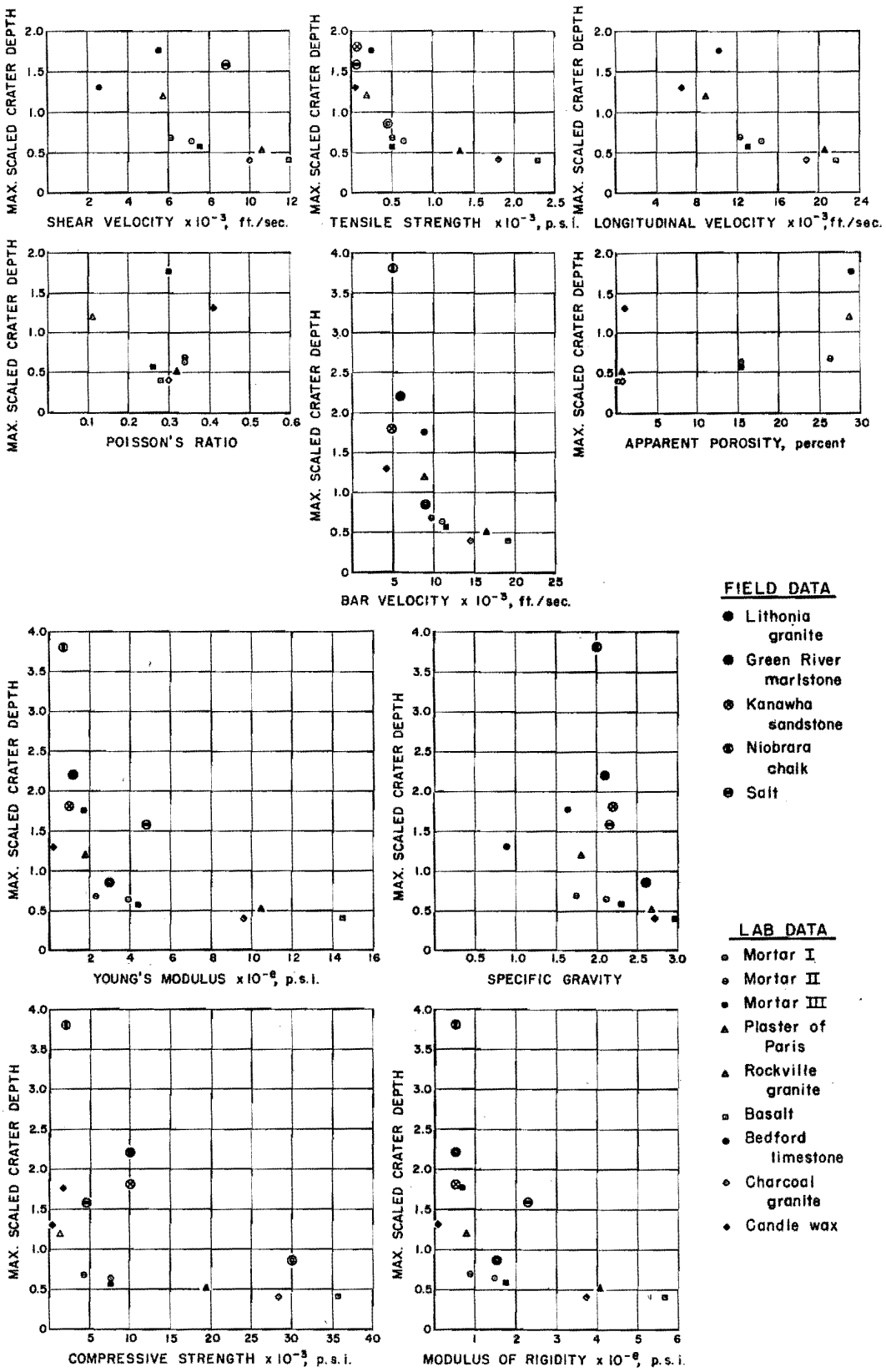

FIGURE 6. - Maximum Scaled Crater Depth vs. Physical Properties. (Scaled crater depth is in ft/lbs$^{1/3}$.

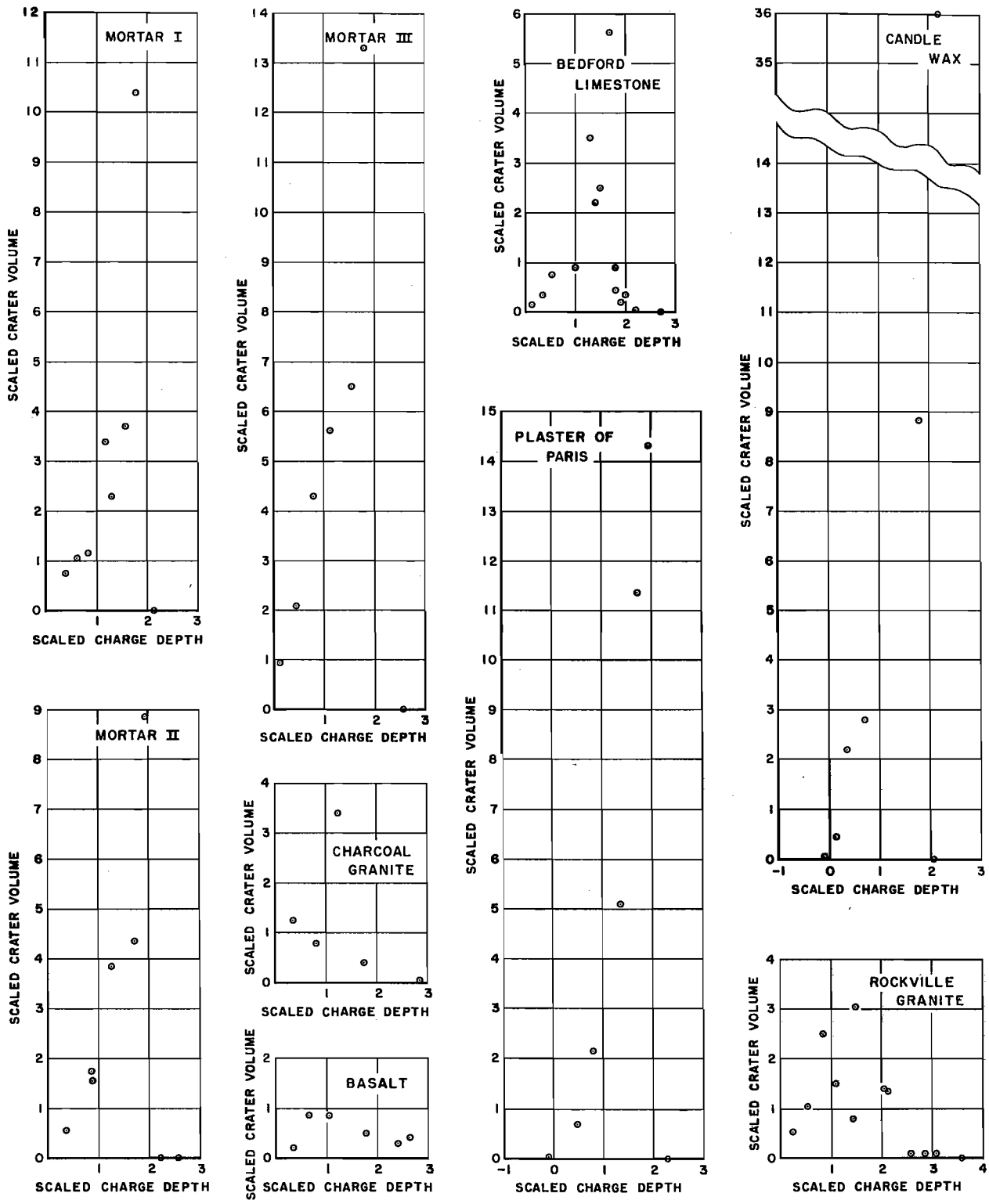

FIGURE 7. - Scaled Crater Volume vs. Scaled Charge Depth. (Scaled crater volume is in ft^3/lbs and scaled charge depth is in $ft/lbs^{1/3}$.

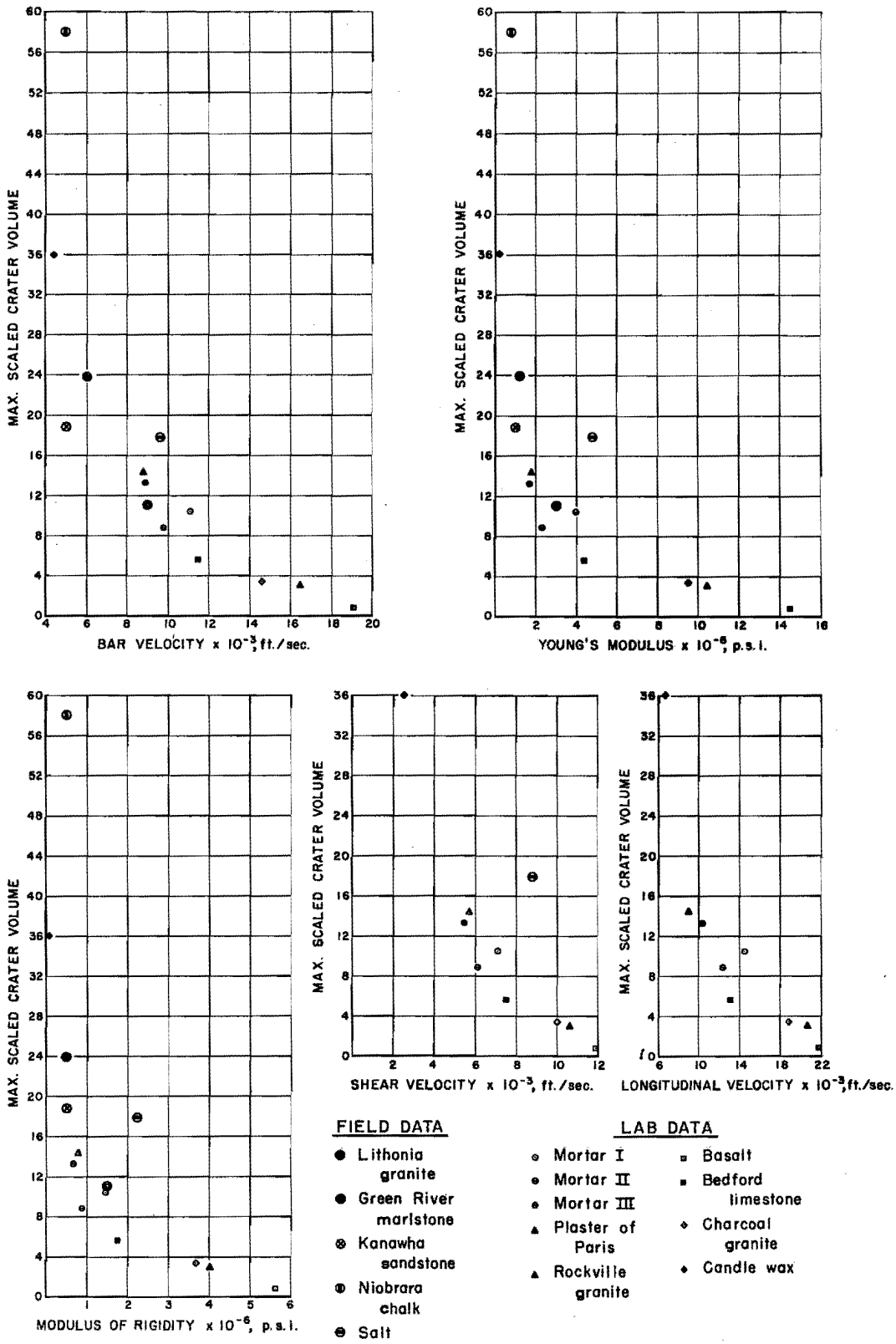

FIGURE 8. - Maximum Scaled Crater Volume vs. Physical Properties. (Scaled crater volume is in $ft^3/lbs.$)

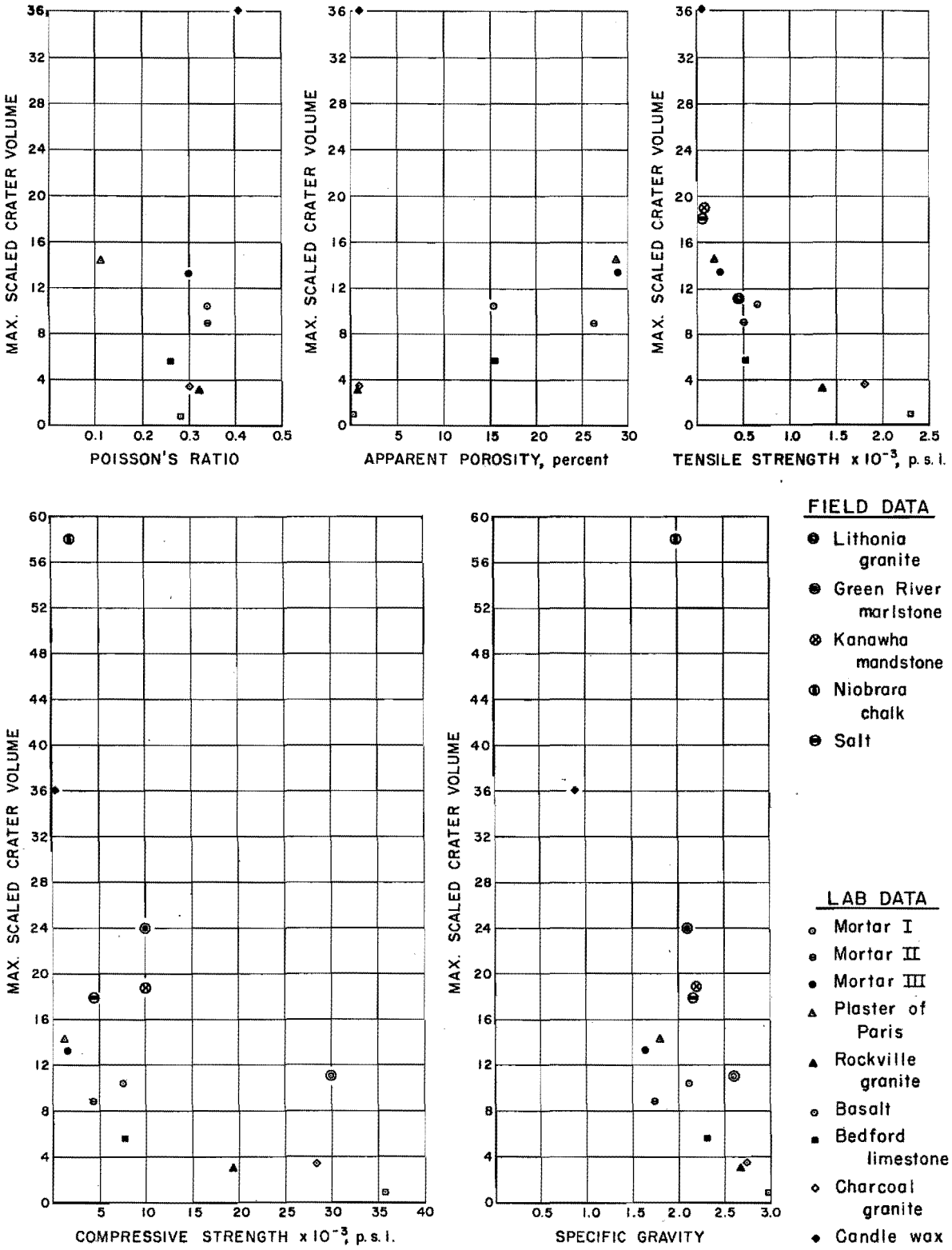

FIGURE 8. - Maximum Scaled Crater Volume vs. Physical Properties. (Scaled crater volume is in ft^3/lbs.) (Con.)

expect the increased scatter shown in these graphs. The tensile-strength plot, however, is still a good one, the field data falling in well with the laboratory data.

Crater Radius

Scaled crater radii versus scaled charge depths are shown in figure 9, and maximum radii as a function of physical properties, in figure 10. As might be expected, the data are similar to the corresponding plots of scaled crater volume. One notable thing is that the largest maximum scaled crater radius is about 4 and that several of the materials are grouped around this value.

Interrelationship of Physical Properties

In order to detect possible trend correlations, the seven measured physical properties were plotted against each other (fig. 11). Nine measurements are hardly sufficient to establish any definite relationships, but certain trends are apparent. The ratio of compressive strength to tensile strength was about 15 for the four rocks tested and ranged from 4 to 12 for the synthetic materials.

CONCLUSIONS

The data presented herein support the conclusion that static tensile strength is related to the maximum scaled crater dimensions obtained by blasting. However, the nature of the relationship limits the practical applicability for use in prediction. Field data are consistent with the laboratory tests in both synthetic material and rock. More scatter occurs between other physical properties and maximum crater dimensions, but trend relationships still exist, with the field data being less consistent.

The limited amount of data presented here also indicates that correlations exist between the mechanical properties themselves. It would be of considerable practical importance if a relationship could be found between tensile strength and elastic wave velocity or compressive strength.

The maximum charge depth at which cratering will occur is not determined by the strength of the material but by pulse attenuation in the material.

The maximum crater depths tend to be more or less constant between scaled charge depths of 0.5 and 2.0, and the maximum scaled crater radius obtainable in any material was about 4.0.

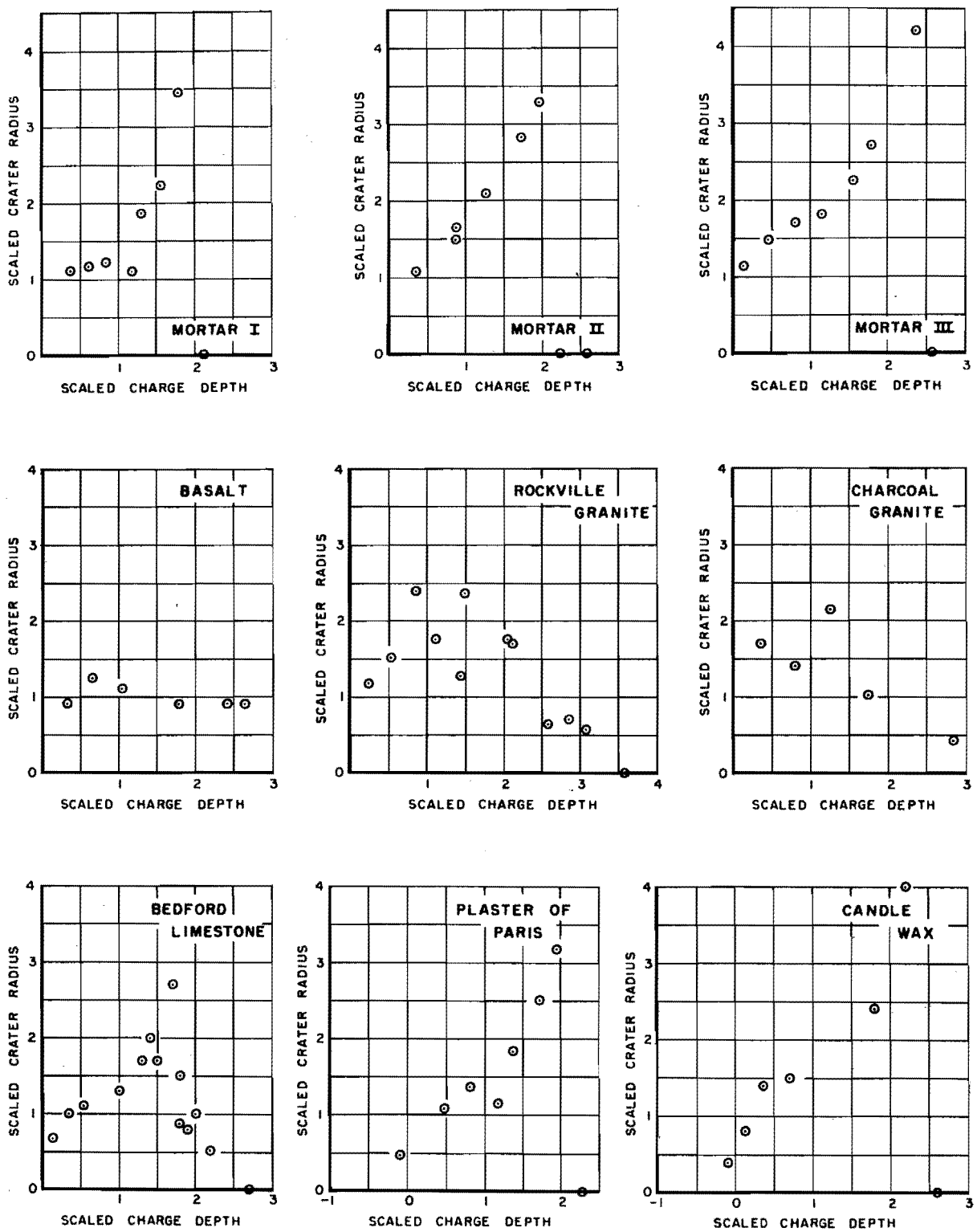

FIGURE 9. - Scaled Crater Radius vs. Scaled Charge Depth.
(Scaled charge depth is in ft/lbs$^{1/3}$.)

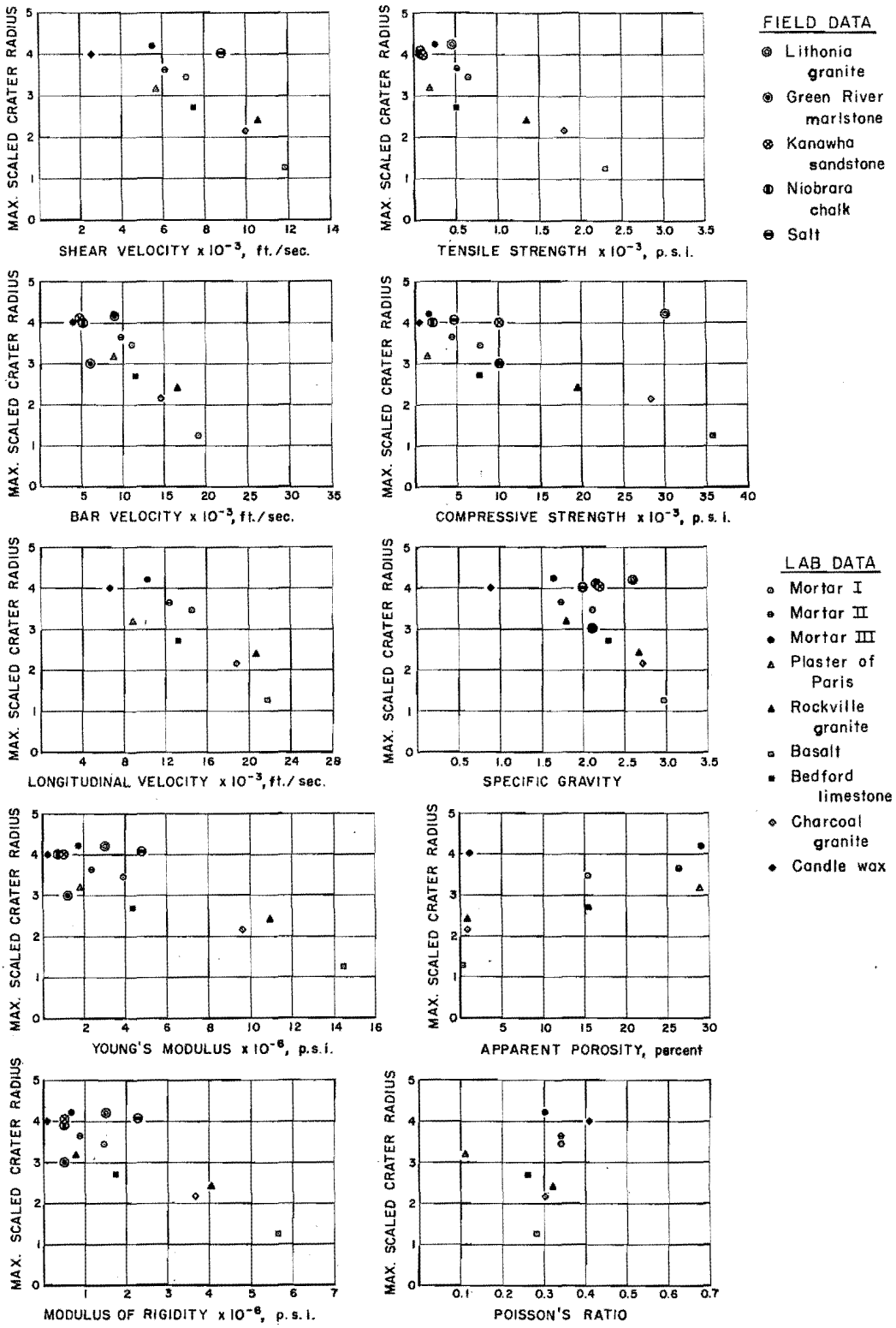

FIGURE 10. - Maximum Scaled Crater Radii vs. Physical Properties.

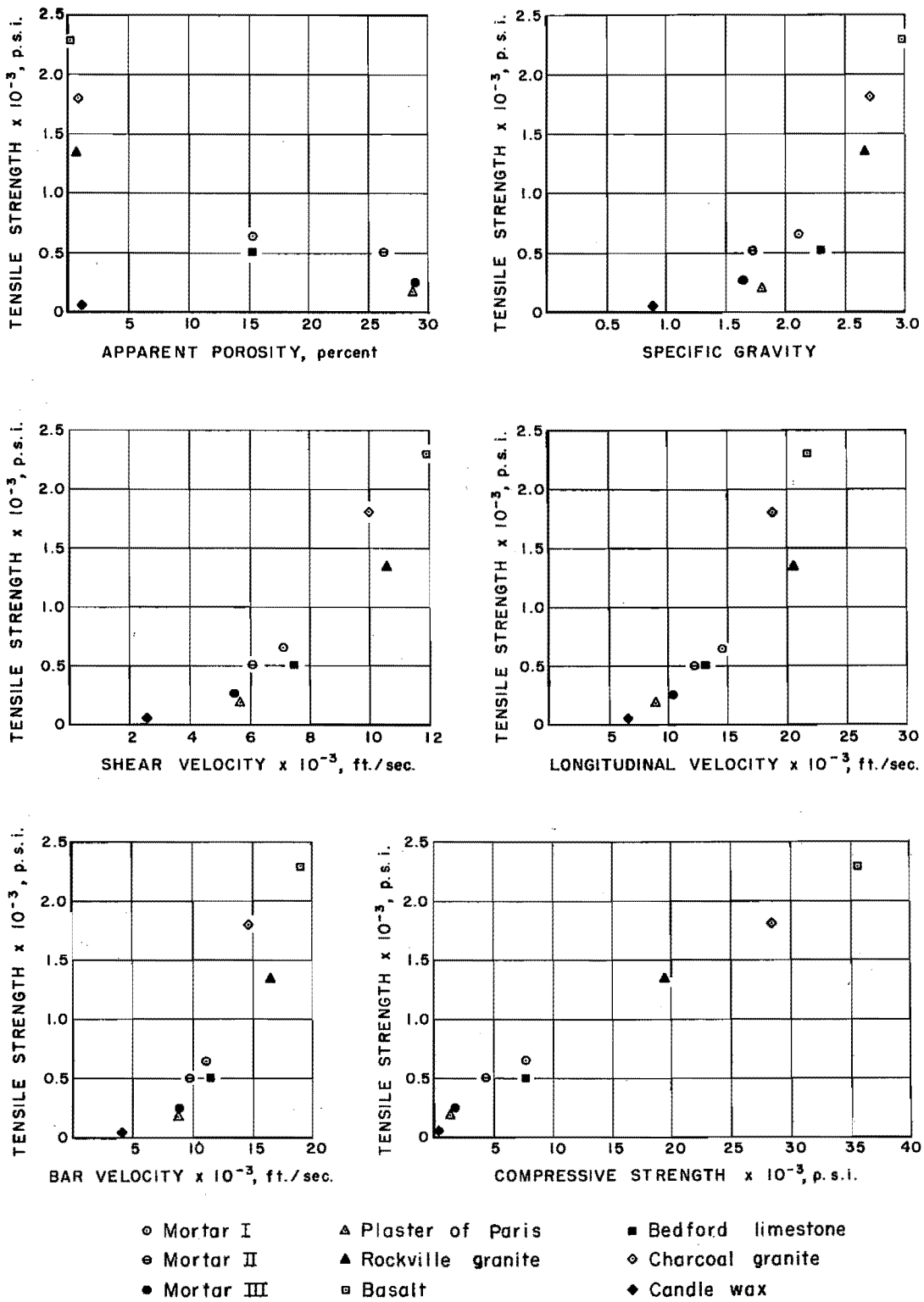

FIGURE 11. - Plots of Measured Physical Properties Against Each Other.

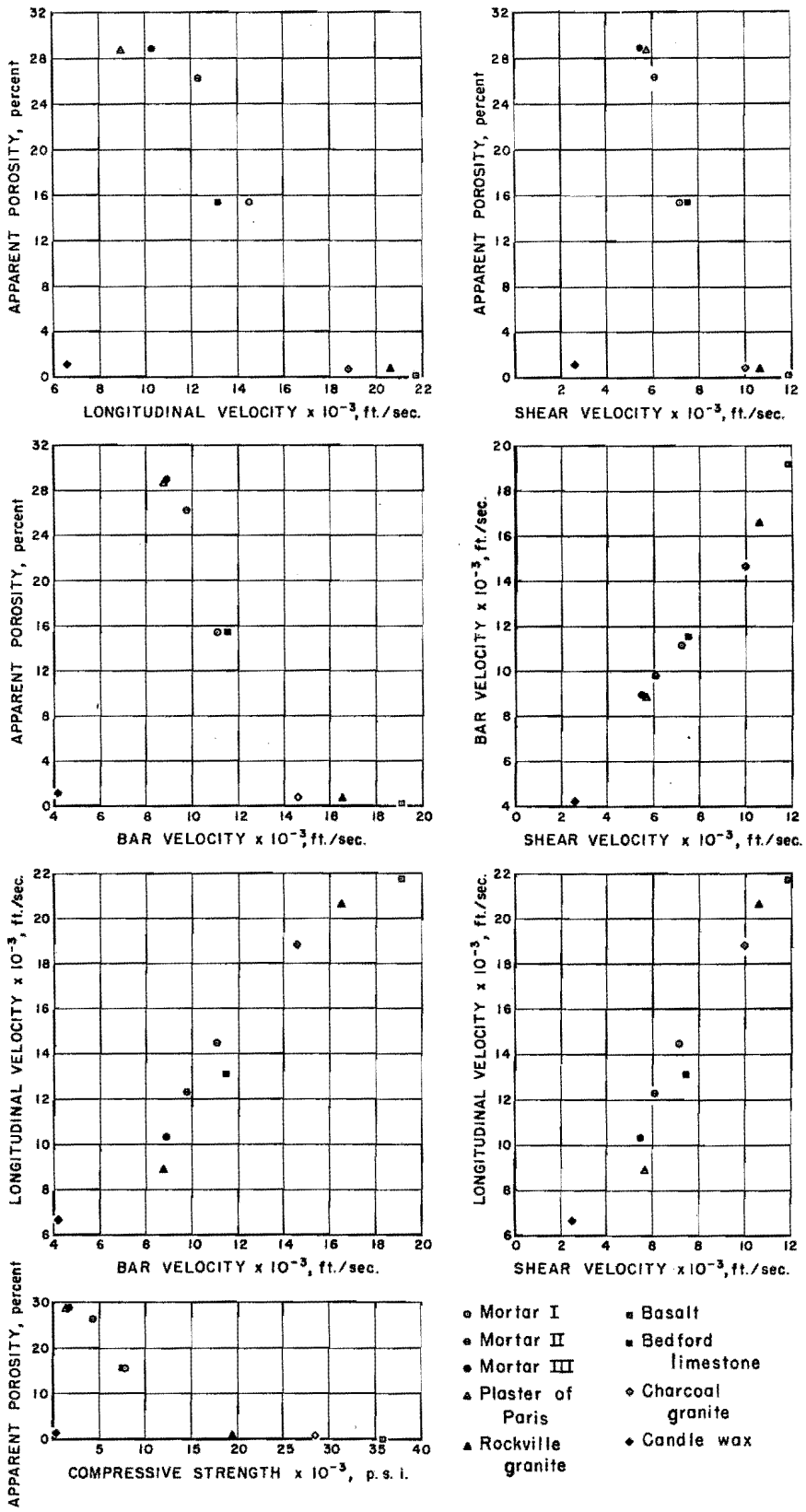

FIGURE 11. - Plots of Measured Physical Properties Against Each Other. (Con.)

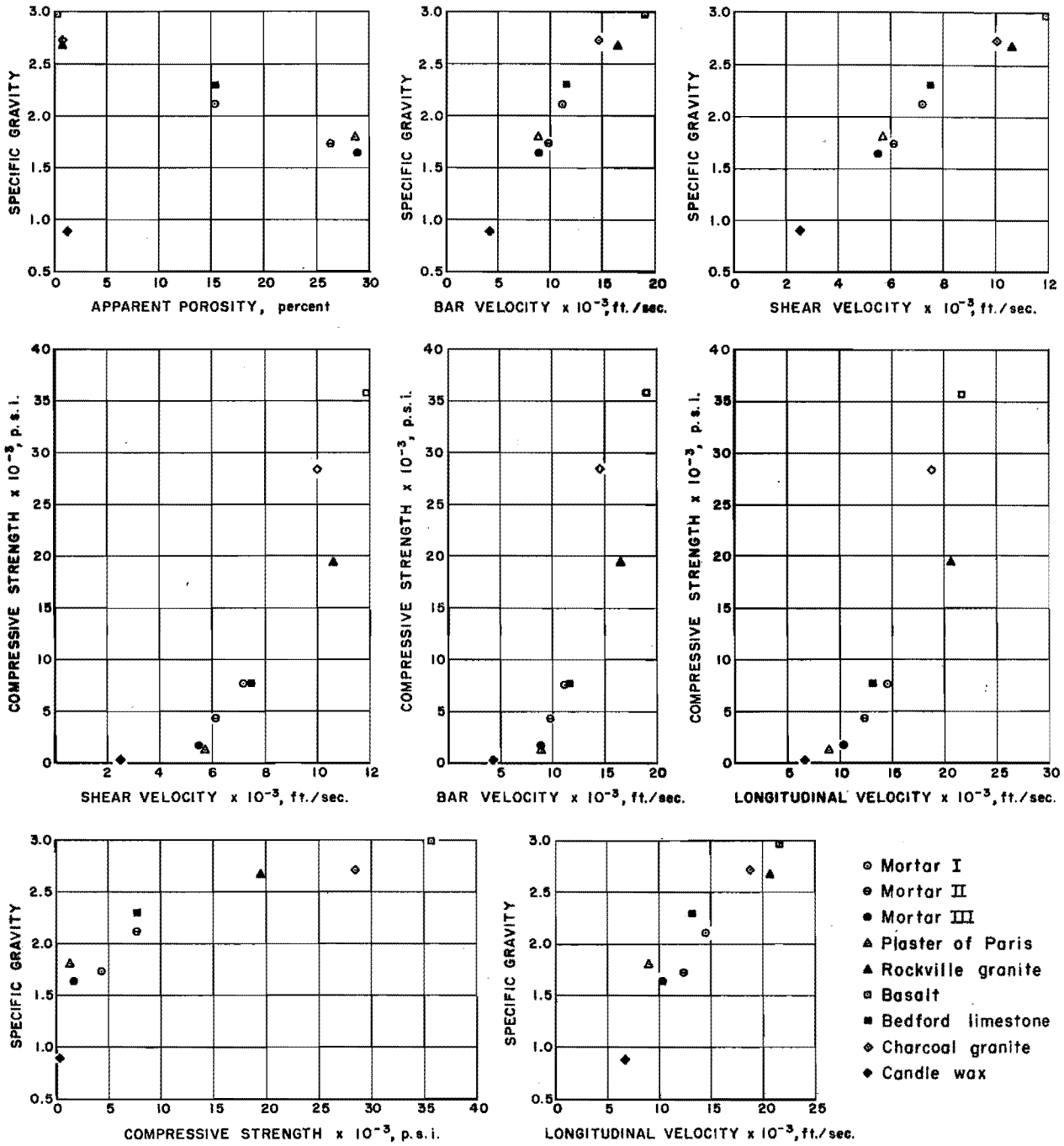

FIGURE 11. - Plots of Measured Physical Properties Against Each Other. (Con.)

REFERENCES

1. Duvall, W. I., and T. C. Atchison. Rock Breakage by Explosives. BuMines Rept. of Inv. 5356, 1957, 52 pp.

2. Johnson, J. Burlin. Small-Scale Blasting in Mortar. BuMines Rept. of Inv. 6012, 1962, 22 pp.

3. Nicholls, H. R., V. Hooker, and W. I. Duvall. Dynamic Rock Mechanics Investigations, Project Cowboy. BuMines Appl. Phys. Res. Lab. Rept. A.P.R.L. 38-3.2, Sept. 1, 1960.

4. Obert, L., S. L. Windes, and W. I. Duvall. Standardized Tests for Determining the Physical Properties of Mine Rock. BuMines Rept. of Inv. 3891, 1946, 67 pp.

5. Reichmuth, D. R. Correlation of Force-Displacement Data with Physical Properties of Rock for Percussive Drilling Systems. Proc. of the Fifth Rock Mech. Symp., Univ. Minnesota, Minneapolis, Minn., May 2-5, 1962.

INT.•BU.OF MINES,PGH.,PA. 4951